26

Semiconducting and Photovoltaic Ferroelectrics

Andrew R. Akbashev[1], Vladimir M. Fridkin[1,2], and Jonathan E. Spanier[1]

[1]*Drexel University, USA*
[2]*Russian Academy of Sciences, Moscow, Russian Federation*

26.1 Introduction

Light–matter interactions in ferroelectric polar materials have attracted attention for decades, driven largely by interest in electronic carrier separation via ferroelectric polarization, observation of anomalously large photovoltages in bulk ferroelectrics, and large optical non-linear susceptibilities. Coupling of light with thin-film electronic materials possessing switchable ferroelectric order is enabling for application of new functionalities, including strain-engineered design of nanoscale ferroelectric domain structure and domain wall variant-dependent electronic and optical properties for manipulating carrier separation resulting in above band-gap voltage output and non-volatile memory based on the ferroelectric photovoltaic effect. Advances, for example, in fundamental understanding of the bulk ferroelectric photovoltaic effect and in optical manipulation of ferroelectric polarization suggest new paradigms for encoding, manipulating, and storing information, optical detection, and sensing that extend well beyond photovoltaic power conversion alone.

In this chapter we review the background and significant advances in the science based on exploiting known and novel light–matter interactions in semiconductor ferroelectrics possessing atomic and mesoscopic-scale degrees of freedom. Novel chemical design strategies for attaining, tuning, and understanding FE and electronic properties through, for example, cation arrangement and cation and O stoichiometry, will be discussed in conjunction with

Nanoscale Ferroelectrics and Multiferroics: Key Processing and Characterization Issues, and Nanoscale Effects, First Edition. Edited by Miguel Algueró, J. Marty Gregg, and Liliana Mitoseriu.

property characterizations that reveal how new materials have desired polar, light-absorbing and other property combinations. Strategies for synthesizing new complex oxides in both bulk and thin-film form, permitting precise control of stoichiometry and oxidation states and using new methods that are manufacturing-scalable, also will be discussed briefly. Recent advances in understanding coupling of light with switchable polar and orbital degrees of freedom with high spatial, spectral, and/or temporal resolution, and with control of surface environment advance the practical possibilities for using ferroelectrics for applications utilizing light. The promising outlook for materials discovery and innovation in, and applications of, semiconducting ferrroelectrics and multiferroics may be further enhanced through materials genomic approaches.

Ferroelectrics, having intrinsically uncompensated dipolar ordering within the crystal structure, have long been known to exhibit various light-mediated effects that appear in polar and non-polar materials, such as the Dember effect and photorefraction. The intriguing interaction of light with ferroelectrics remains an important frontier area, particularly the photovoltaic effect, understanding of which holds promise for gaining additional insight into the behavior of photoexcited carriers and the development of future photovoltaic materials, devices, and their application. The discussion will cover the key aspects of photovoltaics in ferroelectrics and different mechanisms for the photovoltaic effect taking most known or novel and promising ferroelectric materials as examples. First, we survey the historical and fundamental aspects of photovoltaic effects in various ferroelectrics, providing a comparison with well-known semiconductor materials. Next we highlight various chemical approaches to and design aspects of ferroelectric materials, providing a perspective of the existing or expected photovoltaic properties of such ferroelectrics. In the end, we remark on the outlook for this emerging and captivating field of photovoltaic ferroelectrics. This is a rapidly changing and expanding field; the reader is also referred to the definitive monograph on the subject [1] and other reviews on the subject that have been published recently [2].

26.2 Basic Principles of Photovoltaic Effect in Ferroelectrics

In the 1931 Harry Dember described a photoeffect [3], in which a voltage developed between dark and illuminated sides of a crystal. The so-called Dember effect arises from a difference in electron and hole mobilities produced on the illuminated side of a crystal. In contrast, when a crystal is evenly illuminated, the photovoltage can appear as a result of band bending. It has long been known that for a photovoltaic device based on carrier separation due to band bending at an interface or across a crystal between contacts, the maximum photovoltage developed is ultimately limited by its band-gap value. As early as 1946 anomalously large photovoltages (more than five times the band gap) were reported in films of ThS and PbS [4]. Later, Pensak and Goldstein reported very large temperature- and incident optical intensity-dependent photovoltages in CdTe, exceeding 200V [5,6]. Experiments involving illumination of ferroelectric piezoelectric crystals also revealed photovoltages much larger than the band-gap, first reported by Fridkin and co-workers in SbSI [7] and later in $LiNbO_3$ by Glass et al. [8]. The observation of such anomalous behavior in ferroelectrics opened a new venue in the physics of ferroelectric and light–matter interactions, and the phenomenon was named the "bulk photovoltaic effect" (BPVE). In addition

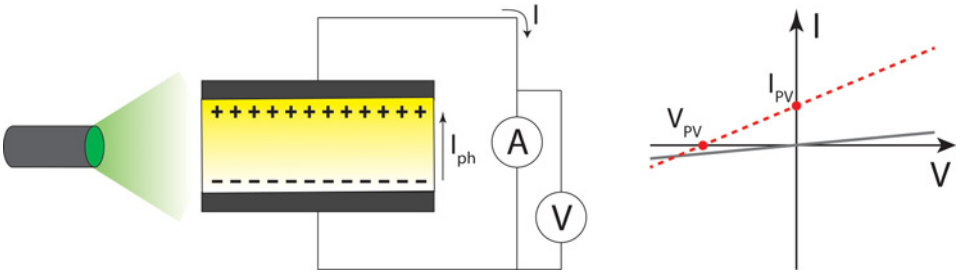

Figure 26.1 *Schematic illustration of a photoexcitation of a ferroelectric by a visible light, which results in the development of an open-circuit photovoltage and a short-circuit photocurrent*

to a large photovoltage that was observed to be invariant with illumination intensity, short-circuited ferroelectric crystals were shown to enter a steady-state photocurrent regime when exposed to homogeneous light, demonstrating a linear dependency on the light intensity [9, 10]. Illustrated in Figure 26.1(a) is the scheme of current–voltage $I(V)$ measurements in a ferroelectric crystal, poled beforehand along the measured current direction. A typical BPVE response in a ferroelectric crystal is illustrated in Figure 26.1(b). Both the dark current and the photocurrent $I_{ph}(V)$ are shown. The intersections of the photocurrent curve with the ordinate is I_{PV}, termed as a photovoltaic current, and with the abscissa is V_{PV}, defined as a photovoltage. Notable is the linear photocurrent-voltage response, markedly different from the rectifying character of diode-based photovoltaics that appears under both dark and light conditions.

BPVE can be observed in crystals which belong to 20 point groups lacking a centre of inversion symmetry (including ferroelectrics and piezoelectrics). For a macroscopic, phemonenological description of the phenomenon, let us consider a ferroelectric crystal in a monodomain state, homogenously illuminated (Figure 26.1). For an open-circuit case, the total current density J_{total} emerging in the crystal is a sum of a photovoltaic current density J_{PV} and the current associated with an induced electric field E_{PV} inside the crystal [1, 9, 11]:

$$I_{total} = I_{PV} + (\sigma_{dark} + \sigma_{ph})\, E_{PV} \tag{26.1}$$

where σ_{dark} and σ_{ph} are dark conductivity and photoconductivity, respectively. The illumination generates electron-hole pairs and, as a result, charges the ferroelectric capacitor, producing an internal electric field E_{PV}. This electric field, in turn, drives the dark current and photocurrent and is responsible for the appearance of the photovoltage V_{PV}:

$$V_{PV} = J_{PV} d/(\sigma_{dark} + \sigma_{ph}) \tag{26.2}$$

where d is the distance between the two oppositely charged surfaces of the ferroelectric crystal. From this expression it is immediately seen that the suppression of both σ_{dark} and σ_{ph} conductivities increases the value of the photovoltage V_{PV}. Thus, one can conclude that for a high photovoltage a ferroelectric should not exhibit high conductivity, while a high photovoltaic current in a ferroelectric, on the contrary, does require good conduction properties. In other words, the photovoltaic efficiency of typical ferroelectrics is mediocre due to small currents on the order of 1 nA cm^{-2}.

Several microscopic mechanisms have been proposed for the BPVE. Glass proposed an asymmetric potential well [12]. Belincher and Sturman proposed asymmetric carrier scattering centers producing net current from randomly drifting carriers [13]. Fridkin has proposed the ballistic mechanism, photoexcitation of non-thermalized carriers with asymmetric momenta and also due to relativistic splitting of the conduction band minimum under polarized light (so-called Dresselhaus or Rashba effect [14]). The hot carriers travel ballistically and descend to the conduction band over a thermalization length. In each of these mechanisms the BPVE can be viewed as a result of different direct and reverse probabilities of electron transitions in k-space due to the non-centrosymmetry of the structure. In a centrosymmetric crystal electron photoexcitations from the valence band or impurity level to the state with the momentum $\boldsymbol{k}$ and $-\boldsymbol{k}$ have equal probabilities. When a crystal lacks inversion symmetry, such probabilities become different, resulting in an asymmetric distribution of electron momenta of photoexcited charge carriers. An alternate model involves the so-called shift mechanism of the BPVE; it is quantum-mechanical in nature, obtained by taking into account the non-diagonal elements of the density matrix. The BPVE in this case is caused not by the carrier movement in the band, but by the shift R in real space following the carrier band-band transition. In these models a key length scales in this process are thermalization length (free path) and the magnitude of the so-called shift vector, corresponding to the length over which entangled carrier-photon non-equilibrium. One of the main drawbacks of using the bulk photovoltaic effect in practical solar energy conversion are impractically small power conversion efficiencies apparently due to the rather weak conducting properties of ferroelectrics and the nature of the bulk photovoltaic effect. Thus, the prevailing view has been the following:

(a) Giant photovoltages are caused by photoexcited charge carriers "separated" by ferroelectric polarization.
(b) The current generated by a giant photovoltage remains very small since the ferroelectric naturally cannot exhibit strong conductivity (as a dielectric).
(c) If the ferroelectric exhibits a high leakage current (better conductivity), its polarization may deteriorate.

In 1981 von Baltz and Kraut proposed a theory for calculating short-circuit photovoltaic current in a pure crystal in terms of its Bloch states and energy bands [15]. Neglecting the effect of photon drag, the short-circuit photovoltaic current can be expressed as:

$$j_{\mathrm{PV}} = G_{ijk} I_0 e_j e_k \tag{26.3}$$

where G_{ijk} is the third-rank photovoltaic tensor (the subscripts ijk refer to the Cartesian coordinate system), I_0 is the illumination intensity, and e_j and e_k are unit vectors describing the electric field components [15]. As can be seen from this expression, the shift current originates from a second-order interaction with light (quadratic with electric field), for which the only requirement is the broken inversion symmetry (ferroelectric polarization may be absent). The shift current tensor couples one or two incident EM fields (each having photon energies larger than the band-gap) of a given linear optical polarization state and incident angle with respect to the ferroelectric polarization, crystallographic plane and collected

current directions. Perturbative analysis of the electromagnetic field classically yields the following expression for the shift current [15–17]:

$$J_q = \sigma_{rsq} E_r E_S \tag{26.4}$$

Here σ_{rsq} links the current density J_q with the electromagnetic field components E_r and E_s and can be expressed as follows:

$$\sigma_{rsq}(\omega) = \pi\ e \left(\frac{e}{m\hbar\omega}\right)^2 \sum_{n',n''} \int d\boldsymbol{k} (f[n''\boldsymbol{k}] - f[n'\boldsymbol{k}])\ x\ \langle n'\boldsymbol{k}\ |\hat{P}_S|\ n''\boldsymbol{k}\rangle$$
$$\times x\ R_q\ x\ \delta(\omega_{n''}(\boldsymbol{k}) - \omega_{n'}(\boldsymbol{k}) \pm \omega) \tag{26.5}$$

where n' and n'' are indexes for the bands, $\boldsymbol{k}$ is the wave vector, and $\omega_n(\boldsymbol{k})$ is the energy of the nth band.

The shift vector R_q is

$$R_q(n', n'', \boldsymbol{k}) = -\frac{\partial \phi_{n'n''}(\boldsymbol{k}, \boldsymbol{k})}{\partial \boldsymbol{k}_q} - [\chi_{n''q}(\boldsymbol{k}) - \chi_{n'q}(\boldsymbol{k})] \tag{26.6}$$

where χ_n are the Berry connections for the band n and ϕ_{nn} is the phase of the momentum matrix element between bands n' and n''. The shift current can be understood as the product of terms depending on (1) the transition intensity, which is proportional to the imaginary part of the dielectric function, and (2) the shift vector, which represents the mean distance traveled by coherent carriers during their lifetimes. Using quantum-mechanical calculations within the density functional theory (DFT) framework, Rappe and Young developed a first-principle approach to the calculation of shift current in ferroelectrics [16, 18]. A striking and consistent agreement between the results of such calculations and the experimental values for $BaTiO_3$ is reproduced, including the difference in sign between the majority of the transverse (xxZ) and longitudinal (zzZ) responses. The calculations reveal a remarkably non-trivial, complex relationship between the shift current and ferroelectric polarization, not evident from Equation (26.5), and this methodology has been applied to the calculation of the shift current in other ferroelectric oxides by these authors, including $BiFeO_3$ [18]. The availability of a DFT approach has opened the possibility of design and simulation of new BPVE materials possessing larger shift current responses and energy conversion efficiencies.

While the shift current is a bulk tensor property that requires non-centrosymmetric (and not necessarily FE) materials, the effect can be more pronounced and it can be manipulated actively through polarization direction, strain, and through materials design in FE materials. For example, the sign of the shift current varies with incident photon energy, incident EM field vector with respect to FE polarization and to collected current directions, and with cation chemistry – even within a group of isostructural FE perovskite oxides of identical symmetry. This enables a new, larger multidimensional parameter space for light-matter coupling with an extraordinary potential for signal encoding and decoding, routing, and manipulation.

26.3 Experimental Evidence of the Bulk Photovoltaic Effect in Ferroelectrics

We next review some of the exemplifying observations of the bulk photovoltaic effect and photocurrent in ferroelectrics. Photovoltaic current in a ferroelectric was first observed in 1955 by A.G. Chynoweth and was proposed to be a consequence of space charge layers at the surface [19]. A single crystal of $BaTiO_3$, *without* an applied electric field, was seen to exhibit pronounced jumps of the electrical current along the polarization direction during illumination, followed by a steady photocurrent state (under no illumination) that was clearly distinct from the pyrocurrent. Afterwards, the photogenerated current was observed in other ferroelectrics, such as $LiNbO_3$ ($LiNbO_3$:Fe) and $KNbO_3$ [8, 20], $LiTaO_3$ [21, 22], SbSI [23], $SbNbO_4$ [24], Pb(Ti,Zr)O_3 [25, 26], $BaTiO_3$ [22, 27], $Bi_4Ti_3O_{12}$ [28], $Sn_2P_2O_6$ [29], $KBiFe_2O_5$ [30], as well as various chemical solutions and heterostructures [31, 32].

26.3.1 $BiFeO_3$

Bismuth ferrite has recently become one of the most notable multiferroics known today [33]. Having a perovskite crystal structure, $BiFeO_3$ has a record-breaking combination of high-temperature ferroelectric ($T_C = 1103$ K) and antiferromagnetic ($T_N = 643$ K) ordering temperatures, and its renaissance began in 2003, after the discovery of a very high ferroelectric polarization (up to 60 μC cm^{-2}, almost ten times higher than for bulk $BiFeO_3$ at that time) at room temperature found in $BiFeO_3$ thin films [34], initially presumed to be the result of an epitaxial strain. Stimulated by the finding, further research confirmed large values of polarization also in single crystals, indicating that proper crystal growth conditions and approaches are required to reduce charge leakage in $BiFeO_3$ and achieve sufficiently robust ferroelectric properties [35].

As a consequence, the first observation of the photovoltaic current in $BiFeO_3$ under visible light illumination was made only in 2009 by Choi et al. [36]. Thin plates of $BiFeO_3$ single crystals, polished down to ∼80–90 μm in thickness, were placed between symmetric Au electrodes and current–voltage ($I(V)$) curves were measured along the polarization with the applied field V being lower than the coercive field of the samples. The experiments demonstrated an intrinsic diode behavior with rather large rectification ratios (159 at 300 K, 488 at 350 K). The diode forward direction appeared to always lie along the FE polarization and could be reproducibly reversed by an application of a polarization-switching electric pulse. In additional to numerous unusual properties, $BiFeO_3$ has one of the narrowest band-gaps of ∼2.7 eV among known undoped oxide ferroelectrics, making it an interesting candidate for investigating the PV effect in ferroelectrics. Illuminated through the semitransparent Au electrodes, $BiFeO_3$ exhibited a steady negative photocurrent without any bias applied. The authors present time dependences of the photocurrents for different light wavelengths at room temperature. The steady-state current under 532 nm excitation reaches ∼7 μA cm^{-2}, while under 630 nm the current has a thousand times smaller value. Such a significant difference in the steady-state current perfectly matches the expectation that the wavelength of 630 nm lies within the sub-band-gap energy region and cannot excite electrons from the valence to the conduction band. The rotation of the polarization plane of the incident light (or the rotation of the $BiFeO_3$ single crystal after fixing the polarization plane of the beam)

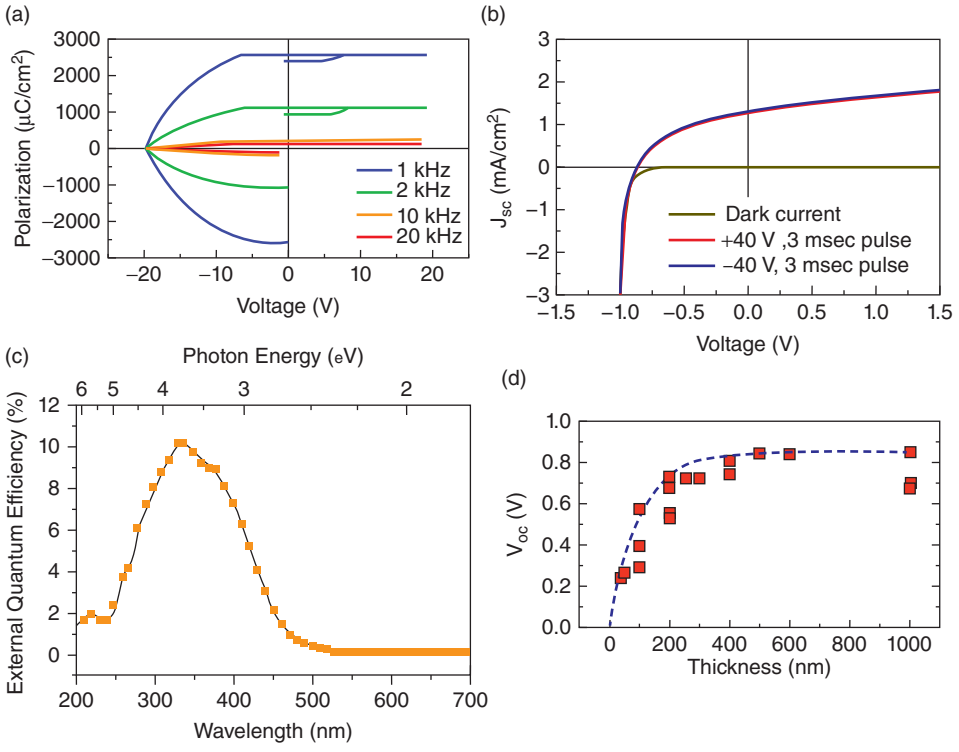

Figure 26.2 *(a) P-E hysteresis loops of the (001)$BiFeO_3$ thin film at different frequencies, (b) I(V) curves in dark and under illumination (2.85 suns) show a photovoltaic effect, and (c) EQE reaches ~10% for the wavelengths close to the corresponding energy of a bandgap. (d) Open-circuit voltage-versus-thickness measurements reveal an interface depletion of 300 nm. Reprinted with permission from [37]. Copyright [2009], AIP Publishing LLC*

caused the photovoltaic current to oscillate concurrently with its maximum corresponding to the light polarization being parallel to the ferroelectric polarization. This sinusoidal behavior was proposed to be the result of a second-order optical response that induces an asymmetric polarization, which in turn is responsible for this optical rectification effect. Further studies of epitaxial $BiFeO_3$ thin films showed that the open-circuit voltages can reach ~16–18 kV cm^{-1} for films thicker than 200 nm with short-circuit current densities of ~1.5 mA cm^{-2} [37]. Figure 26.2(a) and (b) show the corresponding diode-like behavior and photovoltaic effect for $BiFeO_3$ thin films, respectively.

Another important quantity is the *external quantum efficiency* (EQE), which quantifies the photovoltaic current as a function of the incident light wavelength. Such dependence for $BiFeO_3$ is shown in Figure 26.2(c). When the photon energy is larger than the band-gap, the conversion efficiency reaches its maximum of ~10% (the drop in EQE at $\lambda < 325$ nm is due to the light attenuation in the top ITO contact). The authors showed that the diode-like behavior is most likely to be driven by the formation of a Schottky barrier at the $BiFeO_3$–ITO interface, which creates a depletion layer in $BiFeO_3$ with an ionizable impurity density of ~10^{17} cm^{-3} (*p*-type) and a 1.25 eV offset potential. From Figure 26.2(d) it can be see

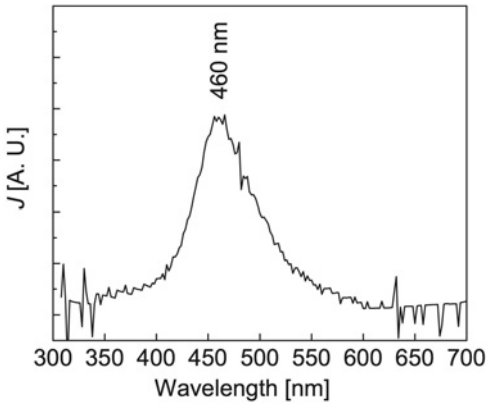

Figure 26.3 *Spectral response for the ITO/$BiFeO_3$(170 nm)/$SrRuO_3$/$SrTiO_3$(001) heterostructure. Reprinted with permission from [38]. Copyright © 2010 Wiley-VCH Verlag GmbH & Co. KGaA, Weinheim*

that the photovoltage saturates to the value of ∼0.8 V when the thickness of the $BiFeO_3$ film is 200 nm and above, providing a further, more rigorous, proof that the depletion layer formation plays a major role in the observed phenomena. In order to clarify whether ferroelectric polarization contributes to the photovoltaic, (111)-oriented $BiFeO_3$ thin films with a strong out-of-plane polarization being in a single-domain state were examined. The photocurrent appeared to be a hundred times smaller than in the case of (001)-oriented films and exhibited a reversible one-order-of-magnitude change upon polarization switching by an applied electric field. The change of photovoltage upon polarization switching, on the other hand, was negligible. In another study of $BiFeO_3$ epitaxial films (170 nm thick) the spectral dependence of photocurrent revealed a peak with a different position as well as a smaller value of photovoltage [38] (see Figure 26.3). In contrast to the previous study where the films were grown by metal–organic chemical vapor deposition (MOCVD), in this case $BiFeO_3$ was deposited by radio-frequency (RF) magnetron sputtering. It is also possible that the difference in preparation methods resulted also in a substantial difference in conductivity: RF-sputtered films demonstrated six orders of magnitude lower conductivity (up to $10^{-12}\ \Omega^{-1}\ cm^{-1}$ at 300 K) when compared to the MOCVD-grown ones, with a dominant conduction mechanism being Schottky emission (the Schottky barrier height is estimated to be ∼0.85 eV). Unexpectedly, such a large difference in conductivity did not lead to a noticeable change in measured photovoltages. It is important to mention, however, that in both works the photocurrent was antiparallel to the FE polarization direction. An interesting point to highlight is that the as-deposited films were a single-domain state and achieved 18 $kV{\cdot}cm^{-1}$. We note here that the development of new, cheaper deposition routes for the growth of $BiFeO_3$ may enable the industrial-scale production of photovoltaic devices utilizing $BiFeO_3$ or other oxide perovskites as an active ferroelectric material. Recently, a manufacturing-scalable technique, atomic layer deposition followed by epitaxial stabilization [39], has been used for the growth of phase-pure $BiFeO_3$ epitaxial thin films with crystalline quality equally high when compared to the $BiFeO_3$ films grown by high-temperature

techniques (PLD, MBE, MOCVD), which are often viewed as being process incompatible with some materials and device technologies.

Further experiments performed on $BiFeO_3$ single crystals at different temperatures added some new insight into the nature of the photovoltaic effect in bismuth ferrite [40]. The samples exhibited much higher conductivity ($\sim 10^{-8}\ \Omega^{-1}\ cm^{-1}$ at 300 K) and the EQE maximum slightly shifted to smaller wavelengths than in the case of the RF-sputtered thin films, which can be attributed to oxygen vacancies. The results suggested that the electrochemical migration of defects such as oxygen vacancies under a large applied electric field as well as switching of ferroelectric polarization are both essential for the switching of the photovoltaic current and the diode rectification direction. In contrast, a different conclusion was drawn from impedance spectroscopic studies of 350-nm-thick $BiFeO_3$ films sandwiched between ZnO:Al and $La_{0.67}Sr_{0.33}FeO_3$ electrodes fabricated by pulsed-laser deposition [41]. The heterostructure showed an increase of the conductivity by at least three orders of magnitude under weak illumination, with the conductivity remaining almost frequency-independent below 1 kHz. In the high-frequency range (above 10 kHz) the conductivity has an insignificant change under light, leading to the conclusion that the photocurrent is electrode–hole assisted (electrode–FE junction, grain-boundary conduction) without previously proposed participation of heavy ions or oxygen vacancies in the conduction.

26.3.2 Niobates

In 1969 F.S. Chen observed the change of refractive indices under light exposure in poled single crystals of ferroelectric $LiNbO_3$ and $LiTaO_3$. The observed photorefraction effect was proposed to be the result of the drifting of photoexcited electrons out from the illuminated area to the dark one, where they were "retrapped"; the electric field developed between the illuminated and dark sides of the crystal caused the observed effect [21]. Apart from spectacular photorefraction change observations, the photocurrent along the *c* crystallographic axis of $LiNbO_3$ was collected under UV illumination (which was perpendicular to the current) under zero applied bias, the resulting time dependence of which is reproduced in Figure 26.4. The detected current was flowing in the direction opposite to the ferroelectric polarization. The transient current was observed to reach a steady state in about

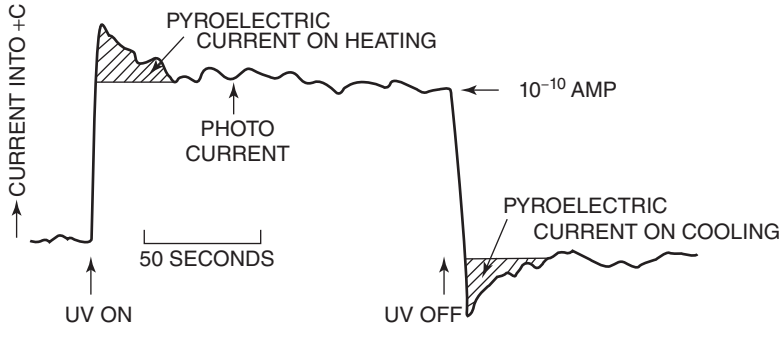

Figure 26.4 *Current-versus-time along the c crystallographic direction of the $LiNbO_3$ crystal when the a face of the crystal was illuminated with a UV light from the mercury discharge lamp. Reprinted with permission from [21]. Copyright [1969], AIP Publishing LLC*

20 s. Later, much effort was devoted to the study of photovoltaic properties of $LiNbO_3$:Fe and $KNbO_3$:Fe crystals, where Fe^{2+} cations are located at the Li^+ and K^+ sites, respectively. From various experiments it became clear that the photocurrent could be observed only along the polar axis of the ferroelectric and is not related to the spontaneous polarization relaxation or pyroelectric effects [8]. When compared to $LiNbO_3$:Fe and $K(Ta,Nb)O_3$, $KNbO_3$:Fe showed a larger photovoltaic effect and photoconductivity, also exhibiting a longer drift length. Spectroscopic studies of absorption constants and photocurrent density of normal (unreduced) and reduced $KNbO_3$:Fe crystals in a short-circuit regime show that the photocurrent is increased for the reduced crystal (Figure 26.5(a)). The absorption peak

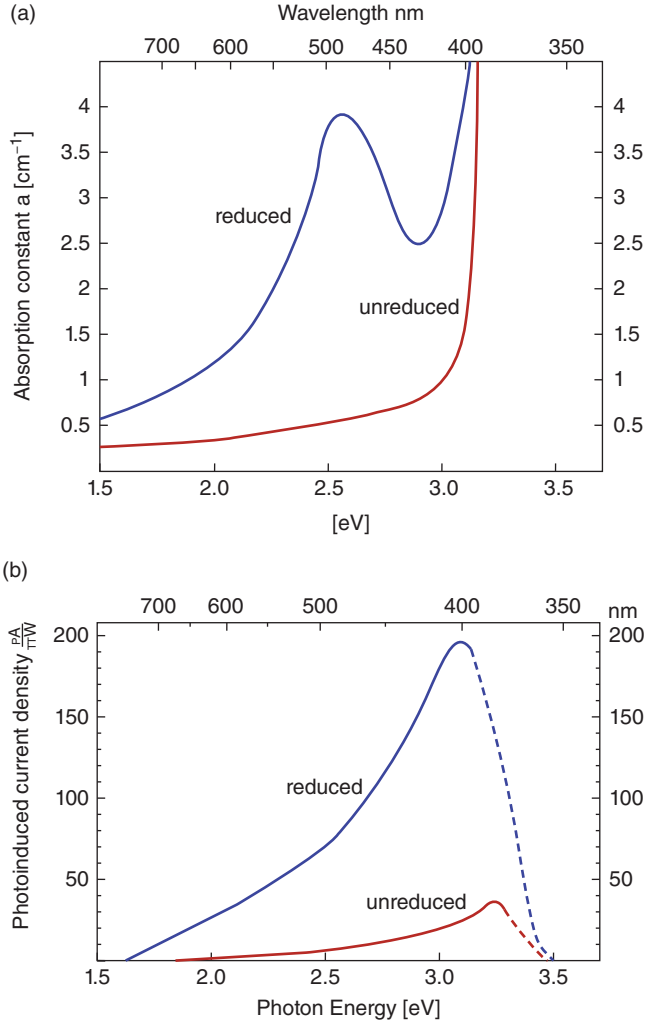

Figure 26.5 *Spectral dependences of the absorption coefficient and photoinduced current density of reduced and unreduced $KNbO_3$:Fe. Reprinted from [20] by permission of the publisher (Taylor & Francis Ltd, http://www.tandf.co.uk/journals)*

at 2.55 eV does not produce a similar increase in the photocurrent, suggesting an inefficient transition of the photorefractive centers of the $KNbO_3$:Fe crystal, similarly to $LiNbO_3$:Fe.

26.4 The Role of the Schottky Barrier and Depletion Layer

The electrodes on both sides of an active ferroelectric layer are typically either metals (Au, Pt, Cu, etc.) or transparent conducting oxides (doped ZnO, ITO, etc.). The photoresponse of the device in this case can be affected by or arise from (a) the formation of a depletion layer (*p–n* junction), (b) electrochemical migration of defects (mainly oxygen vacancies) and the associated change in electronic structure, (c) Schottky emission from metal contacts, and, finally, (d) the bulk photovoltaic effect itself. Therefore, for the correct design and operation of a ferroelectric photovoltaic device it is crucial to understand the physics behind the observed phenomenon, especially in the light of ongoing debate of the mechanisms and their various contributions. Focusing on the study of the FE layer itself, we should keep in mind the fact that an equally careful study of the effect of the electrodes could provide a significant insight into the origin of the photovoltaic effect in many experiments. One of such studies performed by Zhang et al. showed very different photovoltaic responses when different metals were used as electrode materials [42]. The metal/[300 μm (Pb, La)ZrO_3]/ITO heterostructure (both electrodes were 100 nm thick) illuminated by AM1.5 (air mass coefficient) in the experiments exhibited a hundred times higher short-circuit photocurrent J_{sc} and twice as much of an open-circuit photovoltage V_{oc} when the metal electrode was changed from platinum to silver and then to magnesium (Figure 26.6). A significant change of the response with time is of no clear origin, but the authors presume it may be caused by the pyroelectric effect or a slow transport of electrons from the top to the bottom electrode, which seems unlikely. The difference between the work function of a metal contact ($\varphi_{Pt} = 5.5$ eV, $\varphi_{Ag} = 4.26$ eV, $\varphi_{Mg} = 3.66$ eV) and ferroelectric (Pb, La)ZrO_3 ($\varphi_{PLZO} \approx 3.5$ eV), $\Delta\varphi = \varphi_{PLZO} - \varphi_M$, defines the barrier height at the respective interface. As can be seen, the closer φ_M is to φ_{PLZO}, the lower the energy barrier becomes, resulting in a stronger electron emission from the metal contact directly into the FE layer. This is shown in Figure 26.6, which illustrates the energy band diagram of the photovoltaic cell with and without poling: E_{pi} is the polarization-induced internal electric field in an FE layer and E_{bi} is the field coming from the two Schottky barriers close to the top and bottom electrodes, which can deplete the FE layer.

26.5 Photovoltaic Effect Mediated by Ferroelectric Domain Walls

In 1962 Neumark proposed how greater-than-bandgap photovoltages can occur in non-centrosymmetric materials containing stratifications in the form of crystals containing cubic- and hexagonal-segmented polytypes, producing an additive photovoltage and with reversal of sign with wavelength [43]. This photovoltaic mechanism of charge separation realized in ferroelectrics, fundamentally different from the BPVE, was first proposed and demonstrated by Yang et al. in 2010 [44]. In contrast to the BPVE, the new mechanism relies on the FE domain walls situated periodically perpendicular to the current direction. Such a domain wall array can separate charge carriers in a manner not unlike that in multi-polytype crystals as noted above and in classic *p–n* junctions. In the experiment,

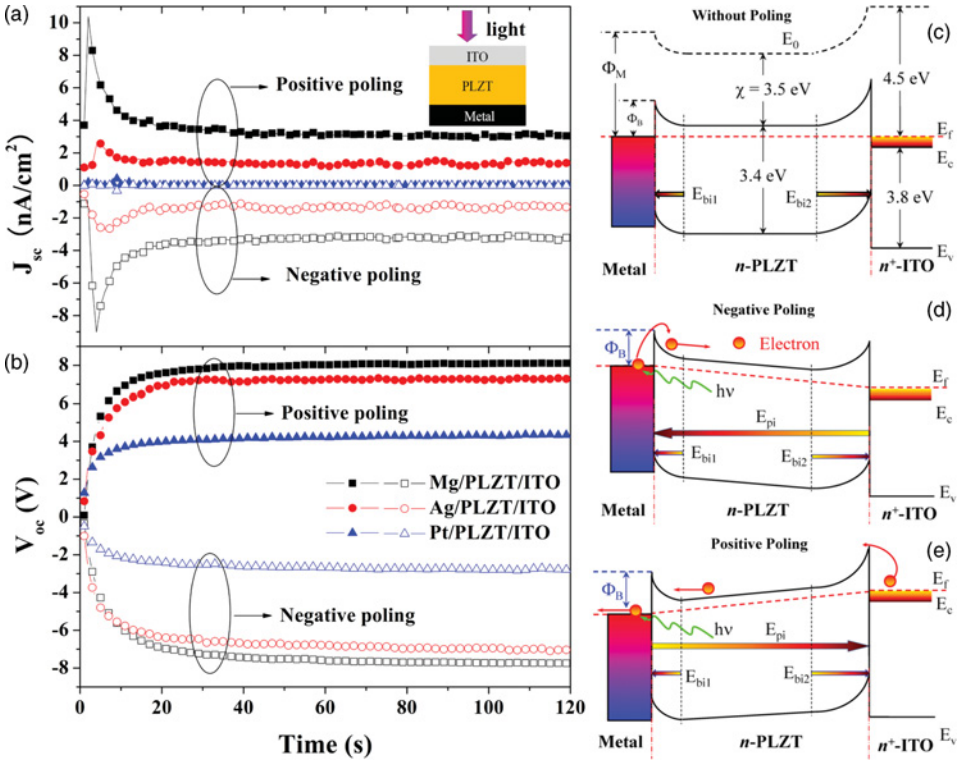

Figure 26.6 *(left) Time dependence of a short-circuit photocurrent density and open-circuit photovoltage of the metal/(Pb,La)ZrO_3/ITO photovoltaic cell. (right) Energy band diagrams corresponding to the unpoled, negatively and positively poled ferroelectric layer in the cell. Reprinted by permission from Macmillan Publishers Ltd: [Scientific Reports] [42], copyright (2013)*

$BiFeO_3$ thin films were deposited on (110) $DyScO_3$ substrates by MOCVD: 71° domain walls appeared in $BiFeO_3$ when it was grown on the substrates annealed in O_2 (1200 °C, 3 h), while 109° domain walls were found in the films on unannealed substrates. The Pt electrodes were deposited on top of the 100-nm-thick $BiFeO_3$ films with an interelectrode distance of 200 μm, with domain walls being either parallel to the measured electrical current or perpendicular to it. The measurements of $I(V)$ characteristics showed an intriguing photovoltaic behavior: a large photovoltage (V_{PV} = 16 V) was observed in the direction perpendicular to the domain walls, but not in the parallel geometry, with a linear dependence on the number of domain walls (Figure 26.7). The absence of a photovoltage both in the parallel direction to the domain walls and for the single-domain sample eliminated the bulk photovoltaic effect as a mechanism for the observed phenomenon.

The proposed mechanism seems conceptually simple and elegant: Each ferroelectric domain wall has a built-in potential that depends on the component of the polarization vector normal to the domain wall, the latter giving rise to the electric dipole in each domain wall. When ferroelectric $BiFeO_3$ is exposed to light, the photogenerated tightly bound excitons require a strong electric field in order to get separated. It turns out that the internal domain wall potential can provide sufficient electric fields needed for the electron–hole

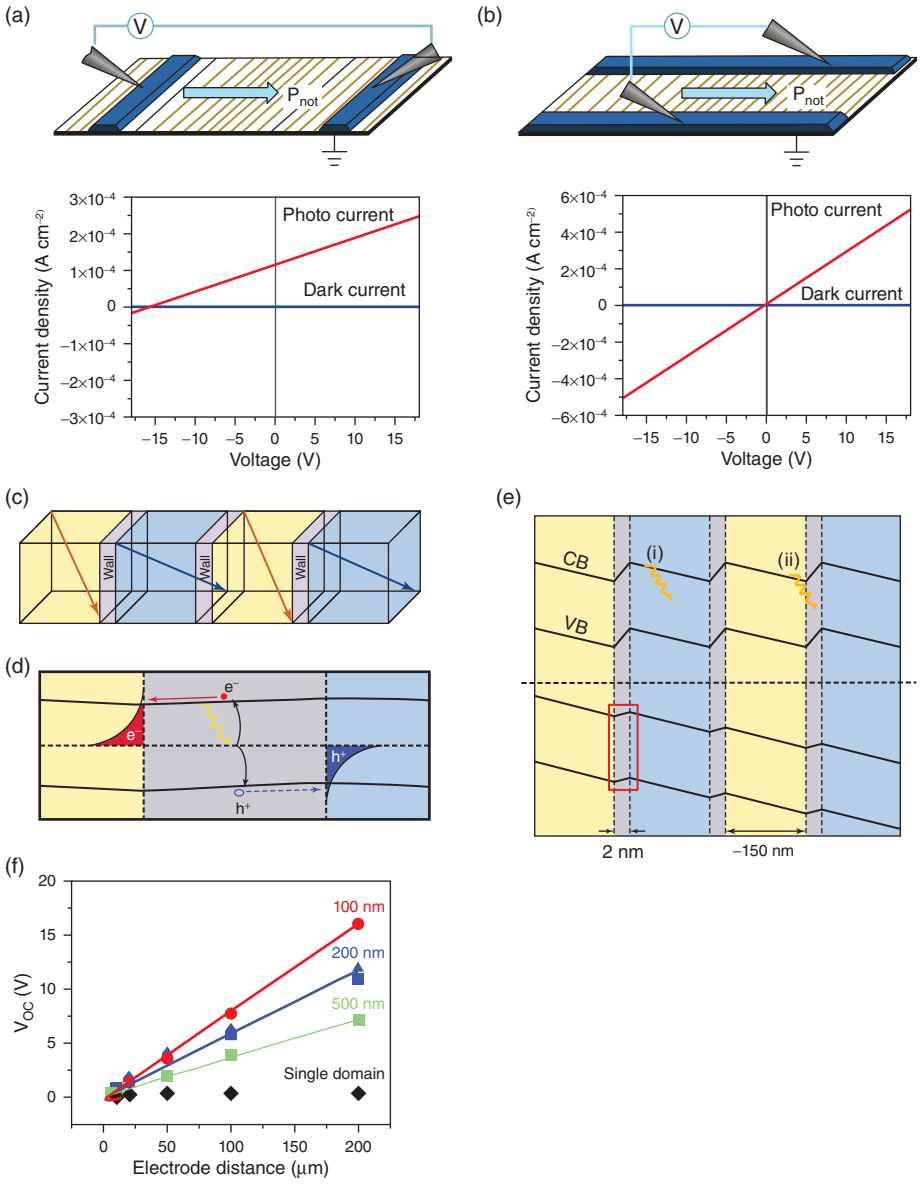

Figure 26.7 *Light and dark I(V) measurements of (a) the perpendicular and (b) the parallel domain wall geometries. (c) Schematic illustration of 71° domains and (d and e) corresponding band diagram across the domain wall (gray). (f) The evolution of open-circuit photovoltage with the distance between the electrodes for the films of different thicknesses (71° domain structure). Reprinted by permission from Macmillan Publishers Ltd: [Nature Nanotechnology] [44], copyright (2010)*

separation. The photoexcited electrons and holes drift to either side of the domain wall (Figure 26.7). This mechanism is in principle similar to the traditional semiconductor *p–n* junction-based solar cell, but with an effective electric field being almost an order of magnitude higher for each domain wall (for the silicon-based junction $V_{PV} = 0.7$ V), greatly overcoming the "band-gap" barrier. The drop of potential at a single domain wall, irrespective of its width, was estimated to be ~10 mV, being close to the predicted value (20 mV) for 71° domain walls in $BiFeO_3$ [45]. Large photovoltage values could also change sign when the ferroelectric polarization is flipped by the application of an electric field (–200 V, 100 μs). A more rigorous description of the proposed mechanism was published later by Seidel and co-workers [46].

A strikingly different observation was made by Bhatnagar et al. in similar $BiFeO_3$ films grown by PLD on (110) $TbScO_3$ [47]. In contrast to the previously described study, large photovoltages were observed for *both types of geometries*, that is domain walls parallel and perpendicular to the measurement direction, with a stronger effect taking place for the parallel orientation of domain walls. An almost exponential increase of the photovoltage value was measured with decreasing temperature to 17 V for 109° domain and 50 V for 71° domain (both at 80 K). Such an unusual behavior of the photovoltaic effect led the authors to suggest that the previously proposed domain-wall-mediated mechanism is incorrect and does not hold a major contribution to the observed photovoltages. Temperature dependences of dark and photo-conductivities (Figures 26.8 and 26.9), on the contrary, can easily explain the exponential increase of V_{PV} with decreasing temperatures. The resistance is lower in the case of perpendicular domain walls because the equivalent circuit is described by $(\sigma_{total})^{-1} = \sum(\sigma_{bulk})^{-1} + \sum(\sigma_{DW})^{-1}$($\sigma_{bulk}$ is the conductivity between the domain walls), while for the parallel domain walls $\sigma_{total} = \sum \sigma_{bulk} + \sum \sigma_{DW}$. It should be remembered that Equation (26.2) shows an inverse proportionality between the conductivity and photovoltage in a material. This simple model also explains why the sample with the 109° domain walls, which are known to be much more conductive than 71° domain walls [48], shows lower photovoltages than the sample with 71° domains. Hence, the authors concluded that for current collected parallel to domain walls, larger-than-bandgap photovoltages can be explained by the BPVE and not the "*p–n* junction"-like accumulation of photovoltage.

26.6 Ferroelectric Solid Solutions: Chemical Tuning of Band-Gap

Because ferroelectrics typically have large band-gaps of more than 3 eV, inefficient absorption of light by such materials leads to their extremely low power conversion efficiency (PCE < 1%) in solar cell applications. Chemical doping of conventional ferroelectric materials has long been a route for introducing higher carrier concentration, spin order, ferroelectric disorder, and better structural stability, and to change various other properties of ferroelectrics. With regard to the field of photovoltaics, chemical substitution enables a tunability of a band-gap of ferroelectrics, especially oxides as most studied ferroelectric materials. In ferroelectric ABO_3 perovskites the electron excitation from the valence band maximum corresponds in a real space to a charge transfer from the oxygen *2p* states to the transition-metal *d* states at the conduction band. Thus, *B*-site partial substitution of typical

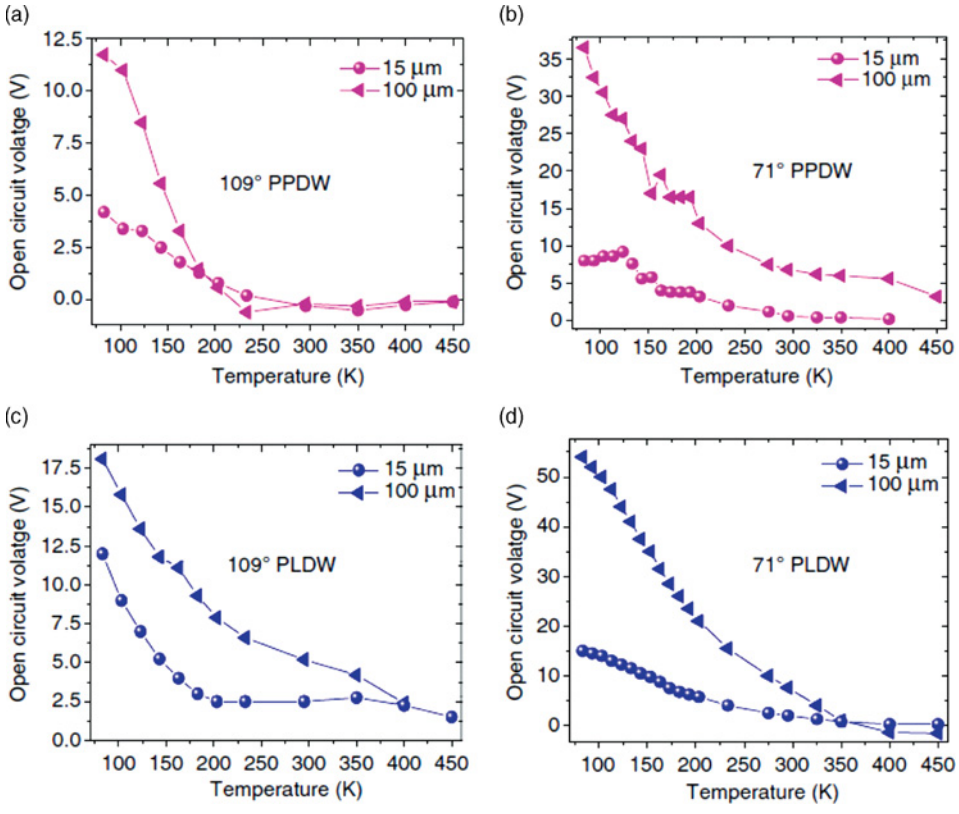

Figure 26.8 *Open-circuit voltage of (100 nm) $BiFeO_3/TbScO_3(110)$ in dark and under light for different domain wall types and orientations (PPDW: perpendicular domain wall, PLDW: parallel domain wall). Reprinted by permission from Macmillan Publishers Ltd: [Nature Communications] [47], copyright (2013)*

ferroelectrics such as $BaTiO_3$, $PbTiO_3$, $BiFeO_3$, and $KNbO_3$ by transition metal ions with filled *d* states could be an effective tool for band-gap tuning in ferroelectrics [49, 50].

The double perovskite Bi_2FeCrO_6, the band-gap of which was originally predicted to be less than 2 eV in a ferromagnetic–ferroelectric state, is particularly interesting [51]. Thin films of (001)-oriented Bi_2FeCrO_6 grown by PLD demonstrated a strong photovoltaic effect along the direction perpendicular to the film surface (Figure 26.10) when the sample was illuminated with a red laser (635 nm, 1.5 mW cm^{-2}) [52]. The film with the thickness of 125 nm grown at $T = 660$ °C (Film *A*) exhibited an open-circuit photovoltage of 0.77 V and a photocurrent of 0.99 mA cm^{-2}, both values being higher than in the case of the film grown at $T = 610$ °C (Film *B*, 0.55 V, 0.11 mA cm^{-2}). The single-wavelength PCE was found to be 6.5% at 635 nm for the sample grown at 660 °C, drastically contrasting with PCE = 0.8% obtained for the film deposited 610 °C. Recently, a PCE of 8.1% was achieved by Nechache et al. in a three-layer FE absorber based on atomic ordering of B-site cations in this same BFCO compound, the largest reported to date for an ferroelectric oxide perovskite. Given the shape of the photocurrent-voltage response, smaller-than-bandgap

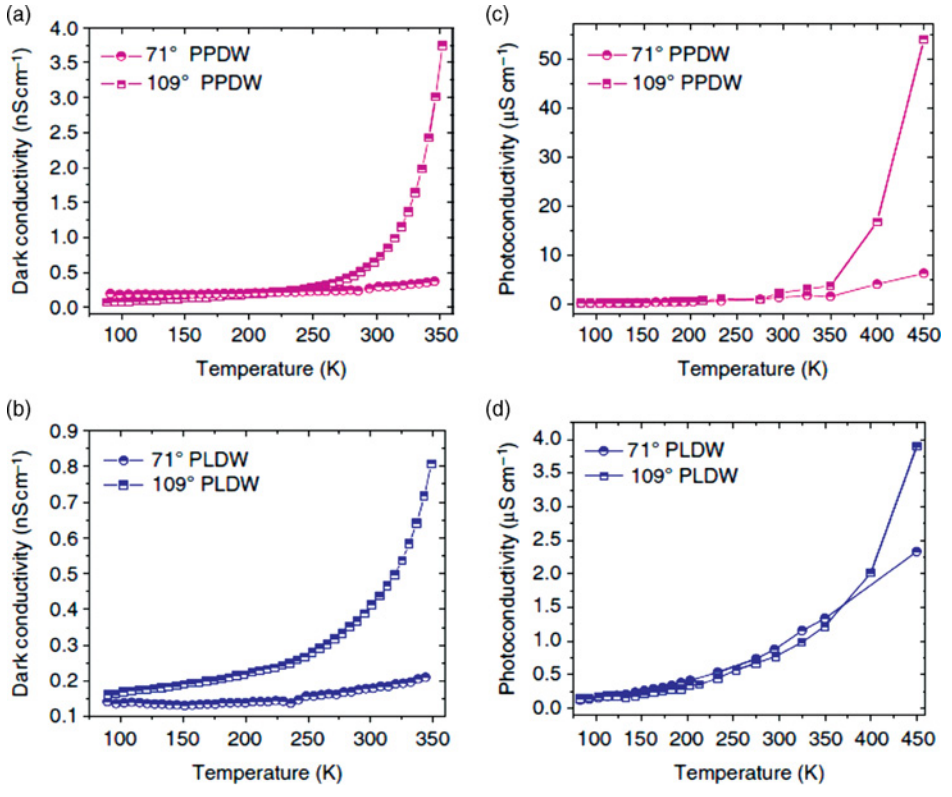

Figure 26.9 *Conductivity measurements of (100 nm) $BiFeO_3/TbScO_3(110)$ in dark and under light for different domain wall types and orientations (PPDW: perpendicular domain wall, PLDW: parallel domain wall). Reprinted by permission from Macmillan Publishers Ltd: [Nature Communications] [47], copyright (2013)*

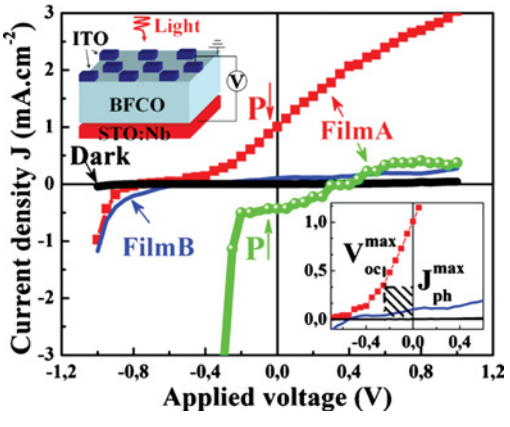

Figure 26.10 *I(V) measurements of (001) Bi_2FeCrO_6 thin films in dark and under light (λ = 635 nm, 1.5 mW cm^{-2}) for different polarization directions. Film A was grown at 660 °C and film B at 610 °C. Reprinted with permission from [52]. Copyright [2011], AIP Publishing LLC. For a color version of this figure, see color plate section*

photovoltage, and dependence of response on ferroelectric-metal band offsets, the dominant mechanism for carrier separation is not likely due to the BPVE, but rather to band bending [53].

Elemental alloying of binary compound semiconductors permits tuning of optical dielectric function and band-gap, band offsets to drive carrier recombination or separation, optical emission characteristics, all with well-developed dopant technology. A significant obstacle to realizing the potential benefits of ferroelectric semiconductors, however, is that ferroelectric oxide perovskites typically possess an inherently large band-gap E_g, typically >3 eV owing to large electronegativity difference between oxygen and transition metal atoms. Ferroelectric stability is driven by selection of *B*-site transition metal cations, representing a significant materials design and synthesis challenge to propose and realize new materials that are robust, and simultaneously narrower-gap, ferroelectric, and have significant compositional tunability.

Despite intense interest in semiconducting ferroelectrics for photovoltaic applications, until recently there were no ferroelectric oxides having a solar-relevant band-gap. The large energy scale of the direct transition of O 2*p* to transition metal *d* has been understood to be a fundamental aspect of perovskite oxides possessing off-center displacements. Recognizing that *B*-site cations drive ferroelectric distortions, introduction of a substitutional *B*-site cation promoting gap narrowing with a classic FE *B*-site cation such as Nb enabled what had been elusive. The solid solution based on ferroelectric $KNbO_3$ was proposed as a small band-gap end member material with a substantial ferroelectric polarization [54]. The introduction of A and B site cation dopants and O vacancies into $KNbO_3$ reduces the experimental band-gap of the parent phase by more than 2 via the formation of Ni^{2+} and oxygen vacancy $V_O^{\bullet\bullet}$, giving rise to the electronic states in the original band-gap of $KNbO_3$, the largest variation in a band-gap for a single family of polar oxides. According to DFT calculations, such $[KNbO_3]_{1-x}[BaNi_{1/2}Nb_{1/2}O_{3-\delta}]_x$ solid solution (KBNNO) should exhibit ~20 μC cm^{-2} at 0 K, which is only twice as small as the polarization of pure $KNbO_3$ at 0 K. Analysis of spectroscopic ellipsometry studies of ceramic bulk KBNNO indicated that the band-gaps of less than 2 eV for $x < 0.5$ and synchrotron X-ray diffraction experiments along with Raman spectroscopy showed that the solid solution with $x < 0.3$ has a tetragonal crystal structure. Photoresponse of the material with $x = 0.1$ peaked at ~700 nm and had a photoresponse "tail" zeroed at 850 nm, enabling an efficient usage of the visible solar spectrum. Ferroelectric switching measurements of the 20-μm-thick pellets confirmed a ferroelectric order with a polarization value of ~15–20 μC cm^{-2} at 77–170 K. Under broad-spectrum lamp illumination the ceramic samples exhibited a photovoltage and a short-circuit photocurrent of 0.7 mV and 0.1 μA cm^{-2}, respectively, with a reversal of the photocurrent direction on change in the sign of the poling voltage. The room-temperature photocurrent in KBNNO was higher than the photocurrent measured for ferroelectrics such as WO_3-doped (Pb, La)(Zr, Ti)O_3 (9 nA cm^{-2} for a 50-μm sample [55]) or (Na, K)(Mg, Nb)O_3 (25 nA cm^{-2} for a 0.84-μm sample [56]) at 300 K. $BiFeO_3$ ceramic pellets (70 μm thick) discussed in the beginning of this chapter exhibited a comparable light response (4 μA cm^{-2} and 30 mV for 10 mW cm^{-2} green-light illumination) [36]. While these results for KBNNO represent a remarkable achievement in their own right, they suggest that strong integration of materials design with solid-state synthesis and thin-film growth, physical, electronic and functional property characterizations and analyses holds great promise for future progress in this area.

26.7 Conclusions

Ferroelectric photovoltaics have long remained a purely academic curiosity. However, in the last decade this area has flourished, attracting an increasing number of materials scientists and engineers. Because FE photovoltaics are currently under intense investigation, within years we anticipate marked improvements in power conversion efficiency of photovoltaic cells based on ferroelectrics, understanding better the origins of high photovoltages observed and new strategies for maximizing photovoltaic current [57–59] and thus bringing further clarification to and impact on this exciting field. In order to create practical FE photovoltaic devices, considerable efforts must be devoted to harnessing the interesting scientific and technological opportunities that can arise through novel theoretical and chemical approaches to photovoltaic ferroelectrics, including understanding the light–matter interaction, new materials design and property simulations, and experimental methods and analyses. Despite great progress, it can be argued that we are entering a new renaissance for ferroelectrics with potential for application in photovoltaic energy conversion and novel optoelectronics.

Acknowledgment

The authors gratefully acknowledge the Materials Science Division of the US Army Research Office under award no. W911NF-14-1-0500 for support.

References

(1) Sturman, B.I. and Fridkin, V.M. (1992) *The photovoltaic and photorefractive effects in non-centrosymmetric materials*, *Vol. 8* in the series Ferroelectricity and related phenomena, Editor: George W. Taylor, Gordon and Breach Science Publishers.
(2) Butler, K.T., Frost, J.M., and Walsh A. (2015) Ferroelectric materials for solar energy conversion: photoferrics revisited. *Energy Environ Sci*, **8**, 838.
(3) Dember, H. (1931) Über eine photoelektronische Kraft in Kupferoxydul-Kristallen (Photoelectric E.M.F. in Cuprous-Oxide Crystals). *Phys. Zeits.*, **32**, 554.
(4) Starkiewicz, J., Sosnowski, L., and Simpson, O. (1946) Photovoltaic effects exhibited in high-resistance semiconducting films. *Nature*, **158**, 28.
(5) Pensak, L. (1958) High-voltage photovoltaic effect. *Phys. Rev.*, **109**, 601.
(6) Goldstein, B. (1958) Properties of Photovoltaic Films. *Phys. Rev.*, **109**, 601–603.
(7) Fridkin, V., Grekov, A., and Malitskaya, M. (1970) Photovoltages in ferroelectric crystal of SbSI type. *Sov. Crystallographic Reports*, **14**, 500.
(8) Glass, A.M., von der Linde, D., and Negran, T.J. (1974) High-voltage bulk photovoltaic effect and the photorefractive process in $LiNbO_3$. *Applied Physics Letters*, **25** (4), 233–235.
(9) Fridkin, V.M. and Popov, B.N. (1978) Anomalous photovoltaic effect in ferroelectrics. *Soviet Physics Uspekhi*, **21** (12), 981–991.
(10) Fridkin, V.M. (1984) Review of recent work on the bulk photovoltaic effect in ferro and piezoelectrics. *Ferroelectrics*, **53** (1), 69–187.

(11) Fridkin, V.M. (2013) Parity nonconservation and bulk photovoltaic effect in a crystal without symmetry center. *IEEE Transactions on Ultrasonics, Ferroelectrics and Frequency Control*, **60** (8), 1551–1555.
(12) Lines, M.E. and Glass, A.M. (1977) Principles and Applications of Ferroelectrics and Related Materials, Clarendon Press, Oxford.
(13) Belincher, V.I. and Sturman, B.I. (1980) The photogalvanic effect in media lacking a center of symmetry. *Sov. Phys. Usp.*, **23**, 199.
(14) Dresselhaus, G. (1955) Spin-orbit coupling effects in zinc blende strcutures. *Phys. Rev.*, **100** (2), 580–586.
(15) von Baltz, R. and Kraut, W. (1981) Theory of the bulk photovoltaic effect in pure crystals. *Physical Review B*, **23** (10), 5590–5596.
(16) Young, S.M. and Rappe, A.M. (2012) First principles calculation of the shift current photovoltaic effect in ferroelectrics. *Physical Review Letters*, **109** (11), art. no. 116601.
(17) Sipe, J.E. and Shkrebtii, A.I. (2000) Second-order optical response in semiconductors. *Physical Review B*, **61** (8), 5337–5352.
(18) Young, S.M., Zheng, F., and Rappe, A.M. (2012) First-principles calculation of the bulk photovoltaic effect in bismuth ferrite. *Physical Review Letters*, **109** (23), art, no. 236601.
(19) Chynoweth, A.G. (1956) Surface space-charge layers in barium titanate. *Physical Review*, **102** (3), 705–714.
(20) Gunter, P. and Micheron, F. (1978) Photorefractive effects and photocurrents in $KNbO_3$: Fe. *Ferroelectrics*, **18** (1), 27–38.
(21) Chen, F.S. (1969) Optically induced change of refractive indices in $LiNbO_3$ and $LiTaO_3$. *Journal of Applied Physics*, **40** (8), 3389–3396.
(22) Brody, P.S. (1981) Photovoltaic and other outputs from pulsed laser illuminated ferroelectrics. *Ferroelectrics*, **38** (1), 939–942.
(23) Fridkin, V.M., Grekov, A.A., Ionov, P.V., et al. (1974) Photoconductivity in certain ferroelectrics. *Ferroelectrics*, 8 (1), 433–435.
(24) Verkhovskaya K.A, Lobachev A.N., Popov, B.N., et al. (1976) The anomalously large photovoltage effect in antimony orthoniobate. *JETP Letters*, **23**, 476–478.
(25) Land, C.E. and Peercy, P.S. (1978) Photoferroelectric effects in PLZT ceramics. *Ferroelectrics*, **22** (1), 677–679.
(26) Lee, J., Esayan, S., Prohaska, J., and Safari, A. (1944) Reversible pyroelectric and photogalvanic current in epitaxial $Pb(Zr_{0.52}Ti_{0.48})O_3$ thin films. *Applied Physics Letters*, **64** (3), 294–296.
(27) Koch, W.T.H., Munser, R., Ruppel, W., and Würfel, P. (1975) Bulk photovoltaic effect in $BaTiO_3$. *Solid State Communications*, **17** (7), 847–850.
(28) Pintilie, L., Alexe, M., Pignolet, A., and Hesse, D. (1998) $Bi_4Ti_3O_{12}$ ferroelectric thin film ultraviolet detectors. *Applied Physics Letters*, **73** (3), 342–344.
(29) Cho, Y.W., Choi, S.K., and Vysochanskii, Y.M. (2001) Photovoltaic effect of $Sn_2P_2S_6$ ferroelectric crystal and ceramics. *Journal of Materials Research*, **16** (11), 3317–3322.
(30) Zhang, G., Wu, H., Li, G.B., et al. (2013) New high T_c multiferroics $KBiFe_2O_5$ with narrow band gap and promising photovoltaic effect. *Scientific Reports*, **3**, art. no. 1265.

(31) Miyazawa, Y., Uchino, K., and Nomura, S. (1982) Bulk photovoltaic effect in the $PbTiO_3$–$La(Zn_{2/3}Nb_{1/3})O_3$ solid solution ceramics. *Ferroelectrics*, **44** (1), 341–347.
(32) Chakrabartty, J., Nechache, R., Li, S., et al. (2014) Photovoltaic properties of multiferroic $BiFeO_3$/$BiCrO_3$ heterostructures. *Journal of the American Ceramic Society*, **97**, 1837–1840.
(33) Catalan, G. and Scott, J.F. (2009) Physics and applications of bismuth ferrite. *Advanced Materials*, **21** (24), 2463–2485.
(34) Wang, J., Neaton, J.B., Zheng, H., et al. (2003) Epitaxial $BiFeO_3$ multiferroic thin film heterostructures. *Science*, **299** (5613), 1719–1722.
(35) Lebeugle, D., Colson, D., Forget, A., and Viret, M. (2007) Very large spontaneous electric polarization in $BiFeO_3$ single crystals at room temperature and its evolution under cycling fields. *Applied Physics Letters*, **91** (2), art. no. 022907.
(36) Choi, T., Lee, S., Choi, Y.J., et al. (2009) Switchable ferroelectric diode and photovoltaic effect in $BiFeO_3$. *Science*, **324** (5923), 63–66.
(37) Yang, S.Y., Martin, L.W., Byrnes, S.J., et al. (2009) Photovoltaic effects in $BiFeO_3$. *Applied Physics Letters*, **95** (6), art. no. 062909.
(38) Ji, W., Yao, K., and Liang, Y.C. (2010) Bulk photovoltaic effect at visible wavelength in epitaxial ferroelectric $BiFeO_3$ thin films. *Advanced Materials*, **22** (15), 1763–1766.
(39) Akbashev, A.R., Chen, G., and Spanier, J.E. (2013) A facile route for producing single-crystalline epitaxial perovskite oxide thinf. *Nano Letters*, **14** (1), 44–49.
(40) Yi, H.T., Choi, T., Choi, S.G., et al. (2011) Mechanism of the switchable photovoltaic effect in ferroelectric $BiFeO_3$. *Advanced Materials*, **23** (30), 3403–3407.
(41) Katiyar, R.K., Kumar, A., Morelet, G., et al. (2011) Photovoltaic effect in a wide-area semiconductor–ferroelectric device. *Applied Physics Letters*, **99** (9), art. no. 092906.
(42) Zhang, J., Su, X., Shen, M., et al. (2013) Enlarging photovoltaic effect: combination of classic photoelectric and ferroelectric photovoltaic effects. *Scientific Reports*, **3**, art. no. 2109.
(43) Neumark, G.F. (1962) Theory of the Anomalous Photovoltaic Effect of ZnS. *Phys. Rev.*, **125** (3), 828.
(44) Yang, S.Y., Seidel, J., Byrnes, S.J., et al. (2010) Above-bandgap voltages from ferroelectric photovoltaic devices. *Nature Nanotechnology*, **5** (2), 143–147.
(45) Seidel, J., Martin L.W., He, Q., et al. (2009) Conduction at domain walls in oxide multiferroics. *Nature Materials*, **8** (3), 229–234.
(46) Seidel, J., Fu, D., Yang, S.Y., et al. (2011) Efficient photovoltaic current generation at ferroelectric domain walls. *Physical Review Letters*, **107** (12), art. no. 126805.
(47) Bhatnagar, A., Chaudhuri, A.R., Kim, Y.H., et al. (2013) Role of domain walls in the abnormal photovoltaic effect in $BiFeO_3$. *Nature Communications*, **4**, art. no. 2835.
(48) Chiu, Y.P., Chen, Y.T., Huang, B.C., et al. (2011) Atomic-scale evolution of local structure across multiferroic domain walls. *Advanced Materials*, **23** (13), 1530–1534.
(49) Qi, T., Grinberg, I., and Rappe, A.M. (2011) Band-gap engineering via local environment in complex oxides. *Physical Review B*, **83** (22), art. no. 224108.
(50) Bennett, J.W., Grinberg, I., and Rappe, A.M. (2008) New highly polar semiconductor ferroelectrics through d^8 cation-O vacancy substitution into $PbTiO_3$: a theoretical study. *Journal of the American Chemical Society*, **130** (51), 17409–17412.
(51) Baettig, P. and Spaldin, N.A. (2005) Ab initio prediction of a multiferroic with large polarization and magnetization. *Appl. Phys. Lett.*, **86**, 012505.

(52) Nechache, R., Harnagea, C., Licoccia, S., et al. (2011) Photovoltaic properties of Bi_2FeCrO_6 epitaxial thin films. *Applied Physics Letters*, **98** (20), art. no. 202902.
(53) Nechache, R., Harnagea, C. Li, S., et al. (2015) Bandgap tuning of multiferroic oxide solar cells. *Nature Photonics*, **9** (1), 61–67.
(54) Grinberg, I., West, D.V., Torres, M., et al. (2013) Perovskite oxides for visible-light-absorbing ferroelectric and photovoltaic materials. *Nature*, **503** (7477), 509–512.
(55) Poosanaas, P., Dogan, A., Thakoor, S., and Uchino K. (1998) Influence of sample thickness on the performance of photostrictive ceramics. *Journal of Applied Physics*, **84** (3), 1508–1512.
(56) Park, J., Won, S.S., Ahn, C.W., and Kim, I.W. (2013) Ferroelectric photocurrent effect in polycrystalline lead-free $(K_{0.5}Na_{0.5})(Mn_{0.005}Nb_{0.995})O_3$ thin film. *Journal of the American Ceramic Society*, **96** (1), 146–150.
(57) Alexe, M. and Hesse, D. (2011) Tip-enhanced photovoltaic effects in bismuth ferrite. *Nature Communications* **2**, 256.
(58) Zenkevich, A., Matveyev, Yu., Maksimova, K., et al. (2014) Giant bulk photovoltaic effect in $BaTiO_3$. *Phys Rev. B* **90**, 161409.
(59) Wang, F., Young, S.M., Zheng, F., et al. (2016) Substantial bulk photovoltaic enhancement by nanolayering. *Nature Communications* **7**, 10419.